Parametric Identification of Chaotic Base-excited Double Pendulum Experimental Study

Y. Liang and B. F. Feeny
Michigan State University
Department of Mechanical Engineering
East Lansing, MI 48824 USA

Abstract

The improved parametric identification of chaotic systems was investigated for the double pendulum system. From recorded experimental response data, the unstable periodic orbits were extracted and later used in a harmonic balance identification process. By applying digital filtering, digital differentiation and linear regression techniques for optimization, the results were improved. Verification of the related simulation system and linearized system also corroborated the success of the identification algorithm.

Keywords: parametric identification, harmonic balance, chaotic system, unstable periodic orbits, double pendulum.

Parametric identification has been a very important method of the construction of mathematical models of vibration systems, theoretically and experimentally. Till now, most of the methods of parametric identification of nonlinear systems focused mainly on free vibration, random excitation or periodically forced steady state vibration behavior (references [1]–[7], etc.). In [1], nonlinear resonances by random excitations are utilized, but only part of the parameters can be identified. Chen and Tomlinson [3] proposed a time series acceleration, velocity and displacement model (AVD model), however with a narrowed investigation scope: dry Coulomb friction, viscous damping and nonlinear stiffness. Also, other methods are effective within limited dynamical systems [4, 5, 6, 7]: weak non-linearity, time-consuming, non-chaotic behavior, or unclear applicability to multi-degree-of-freedom system.

Recently, the application of chaotic behavior in parametric identification has begun to be noticed and some related algorithms were developed. The fundamental property of deterministic chaos is that the chaotic set of a dynamical system contains infinite number of unstable periodic orbits. Furthermore, the approximated periodic orbits can be extracted by phase space reconstruction techniques [8, 9, 10, 11], which can be applied for identification purposes and are of important advantage over a one-periodic-orbit steady state system, since more periodic orbits can usually provide more information of a nonlinear system. The unstable periodic orbits make the identification in chaotic world much simpler. Yasuda et al. [12, 13] introduced an inverse applied harmonic-balance method to estimate parameters. Plakhtienko [14, 15] also introduced a method of special weight function, by which the second order differential equation could be converted to a series of linear equations if some periodic orbits can be known *a priori*. In [14], it is noticeable that if harmonic functions are applied as weighting functions, the rest of the procedure is identical to harmonic balance method. Based on harmonic method, Feeny and Yuan [16] developed a general method for chaotic systems that extracts unstable periodic orbits and then exploits harmonic balance method to predict the parameters. Further more, they [17] applied this technique to an experimental magneto-elastic oscillator; results were accurate and also noise-resistant. The present report is based upon their algorithm. But unlike all of the existed applications, which are single degree of freedom systems, the purpose of this report is to apply and examine the algorithm on a multi-degree-of-freedom system with strong non-linearity.

The work discussed in this report is a further investigation and application of harmonic balance to parametric excited chaotic systems. It includes two parts:

1. simulation verification, which is discussed in detail in the first part of the report [18];

2. experimental verification, which will be introduced in this part of the report.

Simulation results have been very successful in applications to single degree-of-freedom systems. Different types of interpolation or approximation functions have been successfully applied in detecting nonlinear terms in the governing equation of a dynamic system. As for the experimental work, it involves a double pendulum system with parametric excitation, which is strongly nonlinear. Since this double pendulum is a multi-degree-of-freedom one, many new issues showed up in the experiment. Also, some modifications were applied to the identification process in order to extend the theory to the multi-degree of freedom system. Modifications included digital differentiation and other techniques of error reduction.

In the following parts of the report, the system configuration and equations of motion will be described and derived. Then, the method and improvements that were used in the identification will be described. Experimental apparatus and configuration will also be explained. In the last two parts of the report, results will be presented and discussed, and several conclusions were drawn upon discussion.

1 Description of the Double Pendulum System

2 Introduction

A schematic diagram of the double pendulum is shown in Figure 1. The first arm has mass m_1, centroid offset e_1, arm length l_1 ,and angular inertia J_{c1} based upon the arm centroid point. The second arm has mass m_2, centroid offset e_2, arm length l_2, and angular inertia J_{c2}. θ_1 is the absolute angular displacement of the first arm and θ_2 is relative angular displacement of the second arm.

The two arms of the pendulum are supported and connected by low friction bearings. The bearings are assumed to have two types of friction: dry Coulomb friction and viscous damping. To the specific double pendulum that was used in the experiment, tests indicated that the first arm bearings had dominantly Coulomb friction because of no oil lubrication, and the second arm bearings had dominantly viscous friction due to full oil lubrication. With these known properties, we can then obtain the non-dimensional governing differential

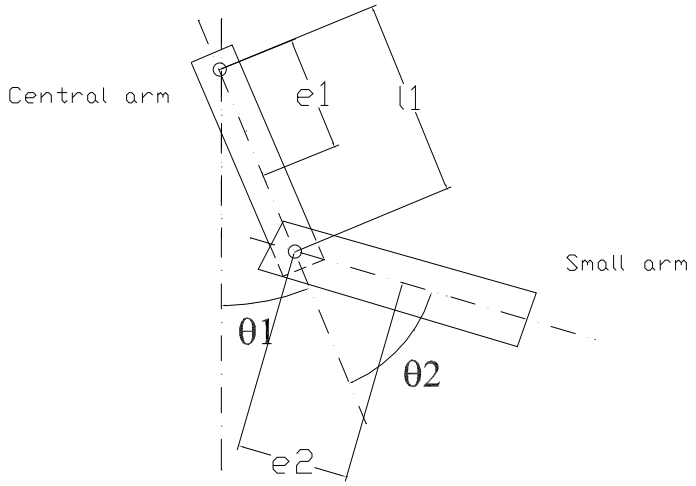

Figure 1: Sketch of the double pendulum.

equations of this system:

$$\begin{cases} \ddot{\phi}_1 + b_{11}\ddot{\phi}_2 \cos(\phi_2 - \phi_1) - b_{11}\dot{\phi}_2^2 \sin(\phi_2 - \phi_1) + b_{12}\sin\phi_1 \\ \qquad +b_{13}\sin\phi_1 \ddot{y} + c_{11} sign(\dot{\phi}_1) - c_{12}(\dot{\phi}_2 - \dot{\phi}_1) = 0 \\ \ddot{\phi}_2 + b_{21}\ddot{\phi}_1 \cos(\phi_2 - \phi_1) + b_{21}\dot{\phi}_1^2 \sin(\phi_2 - \phi_1) + b_{22}\sin\phi_2 \\ \qquad +b_{23}\sin\phi_2 \ddot{y} + c_2(\dot{\phi}_2 - \dot{\phi}_1) = 0 \end{cases}, \tag{1}$$

where $\phi_1 = \theta_1$ and $\phi_2 = \theta_1 + \theta_2$ are absolute angular deflections, $B_{11} = \frac{m_2 e_2 l_1}{J_{o1}}$, $b_{12} = \frac{g(m_1 e_1 + m_2 l_1)}{J_{o1}}$, $b_{13} = \frac{(m_1 e_1 + m_2 l_1)}{J_{o1}}$, $B_{21} = \frac{m_2 e_2 l_1}{J_{o2}}$, $b_{22} = \frac{g m_2 e_2}{J_{o2}}$, $b_{23} = \frac{m_2 e_2}{J_{o2}}$, $c_{12} = \frac{c_{r2}}{J_{o1}}$, $c_2 = \frac{c_{r2}}{J_o 2}$, $J_{o1} = J_{c1} + m_1 e_1^2 + m_2 l_1^2$, and $J_{o2} = J_{c2} + m_2 e_2^2$; y is the excitation displacement of the support with known frequency f_e; and $f(x) = sign(x) = \begin{cases} 1, & x > 0 \\ 0, & x = 0 \\ -1, & x < 0 \end{cases}$ is a sign function representing Coulomb friction . Function $f(x)$ is valid if there are no sticks. For convenience of the analysis, a non-dimensional form of the governing differential equation is desired. By letting $\tau = 2\pi f_e t$ and $\Omega = 2\pi f_e$, then, $\frac{d}{dt} = \frac{d}{d\tau} \cdot \frac{d\tau}{dt} = 2\pi f_e \frac{d}{d\tau} = \Omega \frac{d}{d\tau}$. Under a sinusoidal

excitation $y = a\cos\tau$, where a is the excitation amplitude, equation (1) can be expressed as

$$\begin{cases} \phi_1'' + B_{11}\phi_2''\cos(\phi_2-\phi_1) - B_{11}\phi_2'^2\sin(\phi_2-\phi_1) + B_{12}\sin\phi_1 \\ \quad +B_{13}\sin\phi_1 y'' + C_{11}sign(\phi_1') - C_{12}(\phi_2'-\phi_1') = 0 \\ \phi_2'' + B_{21}\phi_1''\cos(\phi_2-\phi_1) + B_{21}\phi_1'^2\sin(\phi_2-\phi_1) + B_{22}\sin\phi_2 \\ \quad +B_{23}\sin\phi_2 y'' + C_2(\phi_2'-\phi_1') = 0 \end{cases}, \tag{2}$$

where $\phi_i' = \frac{d\phi_i}{d\tau}$, $B_{i1} = b_{i1}$, $B_{i2} = b_{i2}/\Omega^2$ for i=1, 2, $B_{i3} = -b_{i3}a$, $C_{11} = c_{11}/\Omega^2$, $C_{12} = c_{12}/\Omega$ and $C_2 = c_2/\omega$. The differential equation is non-autonomous because of the time dependence of $y(\tau)$.

For identification purpose, the excitation signal y can be approximated by Fourier series expansion of

$$y(\tau) = \sum_{j=1}^{J}(E_j\cos j\tau + F_j\sin j\tau), \tag{3}$$

where the coefficients E_j and F_j are unknown. For the present system with harmonic excitation, $y = E_1\cos\tau + F_1\sin\tau$ is adequate for identification. Since all the parameters are unknown with the only exception of the excitation frequency, equation (2) can then be transformed into

$$\begin{cases} B_{11}\phi_2''\cos(\phi_2-\phi_1) - B_{11}\phi_2'^2\sin(\phi_2-\phi_1) + B_{12}\sin\phi_1 \\ \quad +B'_{13}\sin\phi_1\cos\tau + B'_{14}\sin\phi_1\sin\tau + C_{11}sign(\phi_1') - C_{12}(\phi_2'-\phi_1') = -\phi_1'' \\ B_{21}\phi_1''\cos(\phi_2-\phi_1) + B_{21}\phi_1'^2\sin(\phi_2-\phi_1) + B_{22}\sin\phi_2 \\ \quad +B'_{23}\sin\phi_2\cos\tau + B'_{24}\sin\phi_1\sin\tau + C_2(\phi_2'-\phi_1') = -\phi_2'' \end{cases}, \tag{4}$$

where $B'_{i3} = B_{i3}E_1$ and $B'_{i4} = B_{i3}F_1$ for i=1, 2. For simplicity, we will denote B_{i3} and B_{i4} to replace B'_{i3} and B'_{i4} in the later parts of this report. Equation (4) is then the desired form for identification.

3 Method

The identification process is similar to the one used in the simulation system of parametrically excited single pendulum [18], which contains data acquisition/post-processing, phase plane reconstruction/extracting unstable periodic orbits, formation of the identification matrix and the solution by the least mean square method. Due to some apparatus limitation, some signal noise occurred during digitization. Therefore certain digital filtering techniques were applied to the acquired signals. Details of the post-processing will be introduced in next section. Other modifications are also applied to the double pendulum system for improvement of the identification.

Due to the complexity of the non-linearity of the double pendulum equation (4), our unknown parameters contain only those coefficients of terms of the differential equations, which will greatly simplify the identification matrix. There are totally 11 unknown parameters in the two differential equations, namely, B_{11}, B_{12}, ..., B_{24}, C_{11}, C_{12} and C_2. Similar to the case in [18], the angular displacement θ_1 and θ_2 are variables in S^1 (one dimensional sphere space). However the angular speeds, accelerations and $\sin\phi_i$ (i =1,2) belong to R^1 (one dimensional continuous real space). Hence, for any period k orbit (there may be multiple orbits of same periodicity k, the Fourier series expression of the periodic orbits is

$$\phi_{1,k,l}(t) \approx \Omega_{1,k,l}t + \frac{a_{0,k,l}}{2} + \sum_{j=1}^{m}(a_{j,k,l}\cos\frac{j\omega t}{k} + b_{j,k,l}\sin\frac{j\omega t}{k}) \tag{5}$$

and

$$\phi_{2,k,l}(t) \approx \Omega_{2,k,l}t + \frac{c_{0,k,l}}{2} + \sum_{j=1}^{m}(c_{j,k,l}\cos\frac{j\omega t}{k} + d_{j,k,l}\sin\frac{j\omega t}{k}), \tag{6}$$

where $\Omega_{i,k,l}$, is the average rotation speed per cycle for the lth orbit of period k. By doing so, the following equations can be obtained through the Fourier expansion of periodic orbits:

$$\dot{\phi}_{1,k,l}(t) \approx \Omega_{1,k,l} + \sum_{j=1}^{m}\frac{j\omega}{k}(-a_{j,k,l}\cos\frac{j\omega t}{k} + b_{j,k,l}\sin\frac{j\omega t}{k}), \tag{7}$$

$$\dot{\phi}_{2,k,l}(t) \approx \Omega_{2,k,l} + \sum_{j=1}^{m}\frac{j\omega}{k}(-c_{j,k,l}\cos\frac{j\omega t}{k} + d_{j,k,l}\sin\frac{j\omega t}{k}), \tag{8}$$

$$\ddot{\phi}_{1,k,l}(t) \approx \sum_{j=1}^{m} -\frac{j^2\omega^2}{k^2}(a_{j,k,l}\cos\frac{j\omega t}{k} + b_{j,k,l}\sin\frac{j\omega t}{k}), \tag{9}$$

$$\ddot{\phi}_{2,k,l}(t) \approx \sum_{j=1}^{m} -\frac{j^2\omega^2}{k^2}(c_{j,kl}\cos\frac{j\omega t}{k} + d_{j,k,l}\sin\frac{j\omega t}{k}), \tag{10}$$

$$\ddot{\phi}_{i,k,l}(t)\cos(\phi_{2,k,l} - \phi_{1,k,l}) \approx \frac{e_{1,0,k,l}}{2} + \sum_{j=1}^{m}(e_{i,j,k,l}\cos\frac{j\omega t}{k} + f_{i,j,k,l}\sin\frac{j\omega t}{k}), \tag{11}$$

$$\dot{\phi}^2_{i,k,l}(t)\sin(\phi_{2,k,l} - \phi_{1,kl}) \approx \frac{g_{1,0,k,l}}{2} + \sum_{j=1}^{m}(g_{i,j,k,l}\cos\frac{j\omega t}{k} + h_{i,j,l,k}\sin\frac{j\omega t}{k}), \tag{12}$$

$$sign(\dot{\phi}_{i,k,l}(t)) \approx \frac{p_{1,0,k,l}}{2} + \sum_{j=1}^{m}(p_{i,j,k,l}\cos\frac{j\omega t}{k} + q_{i,j,k,l}\sin\frac{j\omega t}{k}), \tag{13}$$

$$\sin\phi_{i,kl} \approx \frac{r_{1,0,k,l}}{2} + \sum_{j=1}^{m}(r_{i,j,k,l}\cos\frac{j\omega t}{k} + s_{i,j,k,l}\sin\frac{j\omega t}{k}), \tag{14}$$

$$\sin\phi_{i,k,l}\cos t \approx \frac{u_{1,0,k,l}}{2} + \sum_{j=1}^{m}(u_{i,j,k,l}\cos\frac{j\omega t}{k} + v_{i,j,k,l}\sin\frac{j\omega t}{k}), \tag{15}$$

$$\sin\phi_{i,k,l}\sin t \approx \frac{w_{1,0,kl}}{2} + \sum_{j=1}^{m}(w_{i,j,k,l}\cos\frac{j\omega t}{k} + z_{i,j,k,l}\sin\frac{j\omega t}{k}), \tag{16}$$

where k=1, 2, ..., K, and i=1, 2, is the corresponding period of the orbit; K is the maximum periodicity. Meanwhile, for the non-dimensional differential equations, time t here is actually τ in equation (4), and fundamental frequency is 1. If incremental encoders are used to sense the angular displacements, then velocity and acceleration are not directly measured. But, their Fourier transformations can be handily generated by the displacement's Fourier transformation. However, for noise contaminated displacement signals, noisy errors may be amplified in the obtained Fourier spectrum of velocity and acceleration. Also, Fourier series expansions of some terms in the differential equations, such as $\dot{\phi}_{i,k}^2\sin(\phi_{2,k}-\phi_{1,k})$, are not obtained by direct Fourier series expansion of their time domain signal, but by convolution of known Fourier expansion components with a low pass filter applied. The purpose of applying a low pass filter to each signal component before convolution is to avoid noise amplification. Substituting (5–16) into (4), and equating the coefficients of terms with identical harmonic order, we obtain two matrix equations:

$$\begin{pmatrix} e_{2,0,1,1}-g_{2,0,1,1} & r_{1,0,1,1} & u_{1,0,1,1} & w_{1,0,1,1} & p_{1,0,1,1} & \Omega_{1,1,1}-\Omega_{2,1,1} \\ e_{2,1,1,1}-g_{2,1,1,1} & r_{1,1,1,1} & u_{1,1,1,1} & w_{1,1,1,1} & p_{1,1,1,1} & d_{1,1,1}-b_{1,1,1} \\ f_{2,1,1,1}-h_{2,1,1,1} & s_{1,1,1,1} & v_{1,1,1,1} & z_{1,1,1,1} & q_{1,1,1,1} & -(c_{1,1,1}-a_{1,1,1}) \\ \vdots & \vdots & \vdots & \vdots & \vdots & \vdots \\ e_{2,0,k,l}-g_{2,0,k,l} & r_{1,0,k,l} & u_{1,0,k,l} & w_{1,0,k,l} & p_{1,0,k,l} & \Omega_{1,k,l}-\Omega_{2,k,l} \\ e_{2,1,k,l}-g_{2,1,k,l} & r_{1,1,k,l} & u_{1,1,k,l} & w_{1,1,k,l} & p_{1,1,k,l} & d_{1,k,l}-b_{1,k,l} \\ f_{2,1,k,l}-h_{2,1,k,l} & s_{1,1,k,l} & v_{1,1,k,l} & z_{1,1,k,l} & q_{1,1,k,l} & -(c_{1,k,l}-a_{1,k,l}) \\ \vdots & \vdots & \vdots & \vdots & \vdots & \vdots \end{pmatrix} \cdot \begin{pmatrix} B_{11} \\ B_{12} \\ B_{13} \\ B_{14} \\ C_{11} \\ C_{12} \end{pmatrix} = \begin{pmatrix} 0 \\ a_{1,1,1} \\ b_{1,1,1} \\ \vdots \\ 0 \\ \frac{a_{1,k,l}}{k^2} \\ \frac{b_{1,k,l}}{k^2} \\ \vdots \end{pmatrix}, \tag{17}$$

or

$$A_1\vec{x}_1 = \vec{q}_1 \tag{18}$$

and

$$\begin{pmatrix} e_{1,0,1,1}-g_{1,0,1,1} & r_{2,0,1,1} & u_{2,0,1,1} & w_{2,0,1,1} & -\Omega_{1,1,1}+\Omega_{2,1,1} \\ e_{1,1,1,1}-g_{1,1,1,1} & r_{2,1,1,1} & u_{2,1,1,1} & w_{2,1,1,1} & d_{1,1,1}-b_{1,1,1} \\ f_{1,1,1,1}-h_{1,1,1,1} & s_{2,1,1,1} & v_{2,1,1,1} & z_{2,1,1,1} & -(c_{1,1,1}-a_{1,1,1}) \\ \vdots & \vdots & \vdots & \vdots & \vdots \\ e_{1,0,k,l}-g_{1,0,k,l} & r_{2,0,k,l} & u_{2,0,k,l} & w_{2,0,k,l} & \Omega_{1,k,l}-\Omega_{2,k,l} \\ e_{1,1,k,l}-g_{1,1,k,l} & r_{2,1,k,l} & u_{2,1,k,l} & w_{2,1,k,l} & d_{1,k,l}-b_{1,k,l} \\ f_{1,1,k,l}-h_{1,1,k,l} & s_{2,1,k,l} & v_{2,1,k,l} & z_{2,1,k,l} & -(c_{1,k,l}-a_{1,k,l}) \\ \vdots & \vdots & \vdots & \vdots & \vdots \end{pmatrix} \cdot \begin{pmatrix} B_{11} \\ B_{12} \\ B_{13} \\ B_{14} \\ C_2 \end{pmatrix} = \begin{pmatrix} 0 \\ c_{1,1,1} \\ d_{1,1,1} \\ \vdots \\ 0 \\ \frac{c_{1,k,l}}{k^2} \\ \frac{d_{1,k,l}}{k^2} \\ \vdots \end{pmatrix}, \tag{19}$$

or

$$A_2\vec{x}_2 = \vec{q}_2, \tag{20}$$

where $\vec{x}_1$ and $\vec{x}_2$ are vectors of unknown parameters. Given a set of periodic orbits, it is adequate to equate the coefficients of the first several orders of sub-harmonics since they are usually the major components of the periodic orbits and less contaminated by noise. We then truncate the Fourier series expansion, and take the first M orders, such that $M \cdot K > N_c$, where N_c is the number of unknown coefficients in $\vec{x}_1$ or $\vec{x}_2$. With these conditions satisfied, the two equations can be solved by least mean square method:

$$\vec{\tilde{x}}_1 = (A_1^T A_1)^{-1} A_1^T \vec{q}_1 \tag{21}$$

and

$$\vec{\tilde{x}}_2 = (A_2^T A_2)^{-1} A_2^T \vec{q}_2. \tag{22}$$

After the non-dimensional parameters are identified, the physical properties can then be restored according to non-dimensional parameters' definition if part of the physical parameters can be known prior to identification. In the experiment, m_2, e_2, l_1 were treated as known since these physical properties were easily evaluated. Also, by defining $B_{i5} = \sqrt{B_{i3}^2 + B_{i4}^2}$, i=1, 2, we can obtain

$$p_b = |B_{i2}/B_{i5}| = \frac{g}{(2\pi f_e)^2 a}. \tag{23}$$

Hence p_b is a constant for a constant excitation amplitude a and can be used as an indicator of the correctness and accuracy of the identified results.

4 Experiment Description

Figure 1 shows sketch of the double-pendulum that was used in the experiment. Two optical encoders (US digitals) were separately attached to the central arm (first arm) and the

second arm to measure the relative angular displacements θ_1 and θ_2. Both of the encoders have a resolution of 1024, which is capable of detecting a minimum angular difference of 0.3516^o. The two encoders sent out TTL square waves, which are noise-resistant. The TTL signals were then sent to two EDAC (Encoder Digital to Analog Converter) converters, which transformed the TTL waves into analogue signal. After that, a data acquisition terminal translated all the signals into computer-acceptable digital signals.

Table 1: Physical properties of the double pendulum.

m_1 (kg)	0.1362	m_2 (kg)	0.040
e_1 (m)	0.0127	e_2 (m)	0.0267
l_1 (m)	0.0635	l_2 (m)	0.0534
J_1 (kg×m^2)*	5.99×10^{-4}	J_2 (kg×m^2)*	4.033×10^{-5}
C_{11} *	1.01×10^{-3}	C_1 *	0.0485
C_2 *	0.00366	–	–

For validation purpose, Table 1 lists all the physical properties of the double pendulum. The '*' marks in the table denote that some properties are not directly measured, but estimated from other dynamic methods, which implies that those parameters could have small errors. To estimate the mass moment of inertia, a small amplitude free vibration was tested on the double pendulum. By evaluating the two natural frequencies of the system through the FFT, the mass moment of inertia values were calculated. Some parameters related to sampling and experimental setting are listed in Table 2.

Table 2: Experimental settings.

Sampling rate (f_s)	500 Hz	**Excitation freq.** (f_e)	5 Hz
Cut-off freq. (f_c)	80 KHz	**Excitation amplitude** (a)	1.15 cm

With all these settings, the acquired chaotic data was obtained during a 3-hour-long chaotic vibration. The data section lasted 22 minutes.

5 Result and Validation

5.1 Phase plane reconstruction & UPO extraction

For simplicity, the number of embedding dimensions was chosen to be four, e. g. $\theta_1(t)$, $\theta_1(t + dt)$, $\theta_2(t)$, and $\theta_2(t + dt)$. This simplification has been proved to be successful for identification. So then, the remaining question of the phase plane reconstruction was deciding time delay T_d. Mutual information [11] of the signal can be used for choosing adequate time delay.

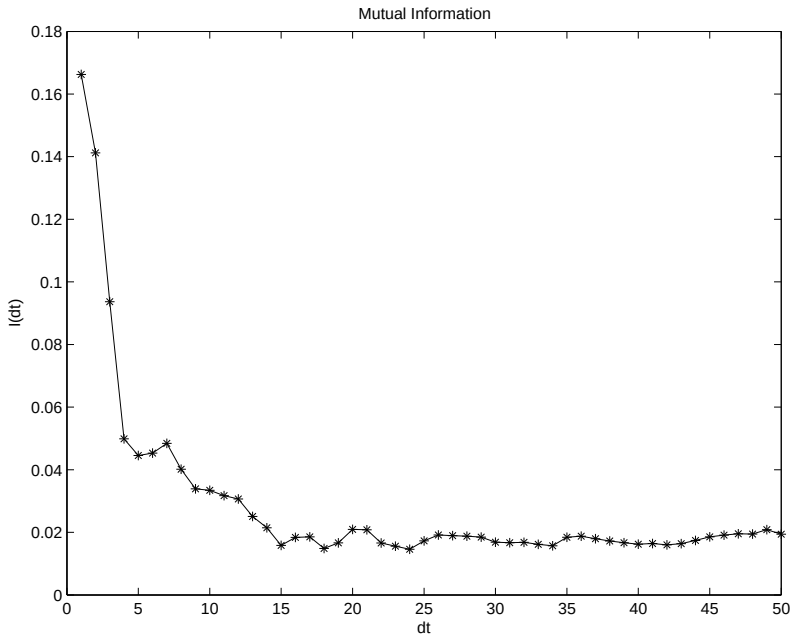

Figure 2: Mutual information $I(dt)$.

It can be seen from Figure 2 that there are weak minima of $I(dt)$at dt =5, 15, 18 and 24. But, T_d=24 in a driving period of 100 samples is somewhat close to a quarter period, the ideal delay for a sinusoidal signal. The reconstructed phase portrait is plotted in Figure 3 with $T_d = 24$. The portrait shows that the central arm represented by θ_1 oscillated in small angles most of the time with occasional large angle whirling, which implies relatively larger noise in θ_1 signal due to the limitation of the optical encoders. Whereas, the second arm displacement, represented by θ_2, consisted mainly of whirling vibration.

After choosing embedding dimensions and time delay, we used the reconstructed phase plane to extract unstable periodic orbits (UPO). Since there are two angles involved, each with different characteristics, the error tolerance of extraction e was to be 5%. Suppose the

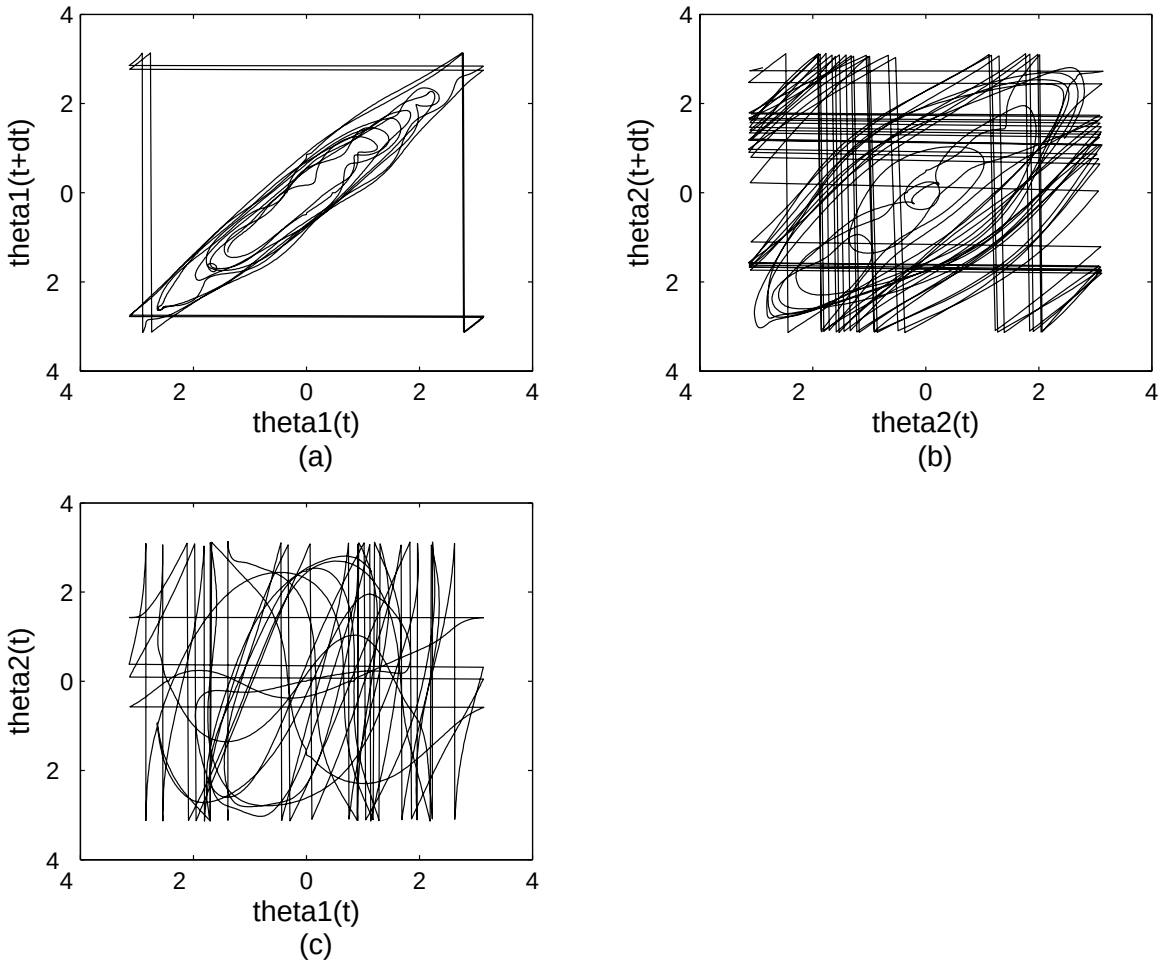

Figure 3: Phase portrait of experimental data with dt=24, **a** $\theta_1(t)$–$\theta_1(t+dt)$, **b** $\theta_1(t)$–$\theta_2(t)$, **c** $\theta_2(t)$–$\theta_2(t+dt)$; θ is represented by theta in the figure.

sampled signal is $s_i(t) = [\theta_i(t) \quad \theta_i(t+T_d)]$ for i=1, 2, an approximated UPO with error tolerance e is extracted if

$$\|s_i(t) - s_i(t+kT)\| < e_i, i = 1, 2, \tag{24}$$

where T is the excitation period and k is periodicity of the recurrence. For the given experimental settings, f_s=500Hz, f_e=5Hz, T=f_s/f_e=100. Then, for example, for a given $k = 4$, if inequality (24) is satisfied, a period 4 orbit is then said to be extracted. One data set of 670,000 points was used in analysis. For a 5% tolerance, 6 distinct orbits were extracted.

Figures 4–9 show the extracted UPOs. In all of the cases, the small arm whirled. In Figure 5 and 7, the central arm whirled, whereas, in other figures, the central arm oscillated

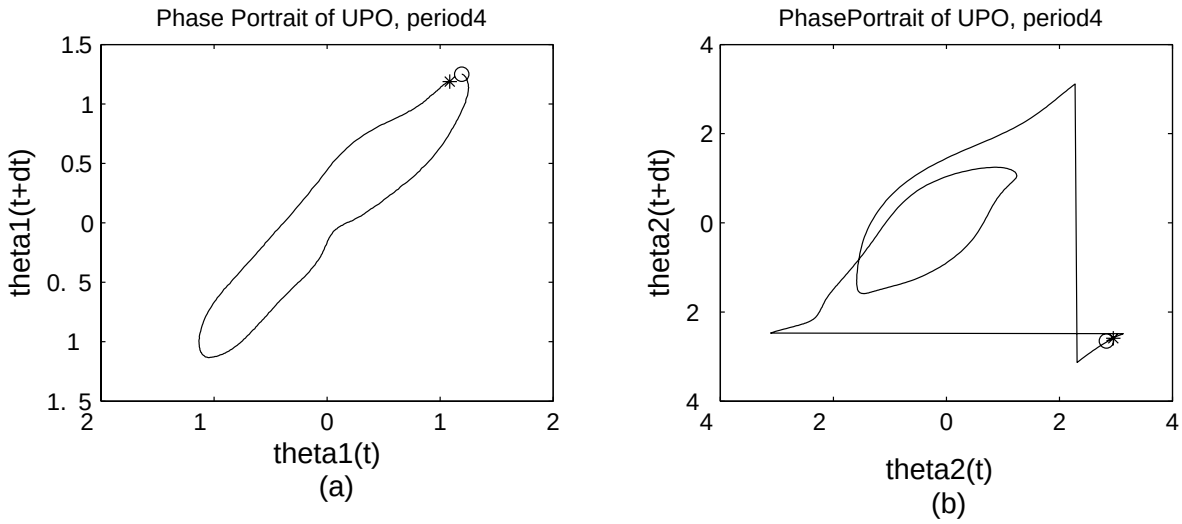

Figure 4: A period 4 UPO; theta1 and theta2 in the plot represent θ_1 and θ_2; dt=24; same for the following figures.

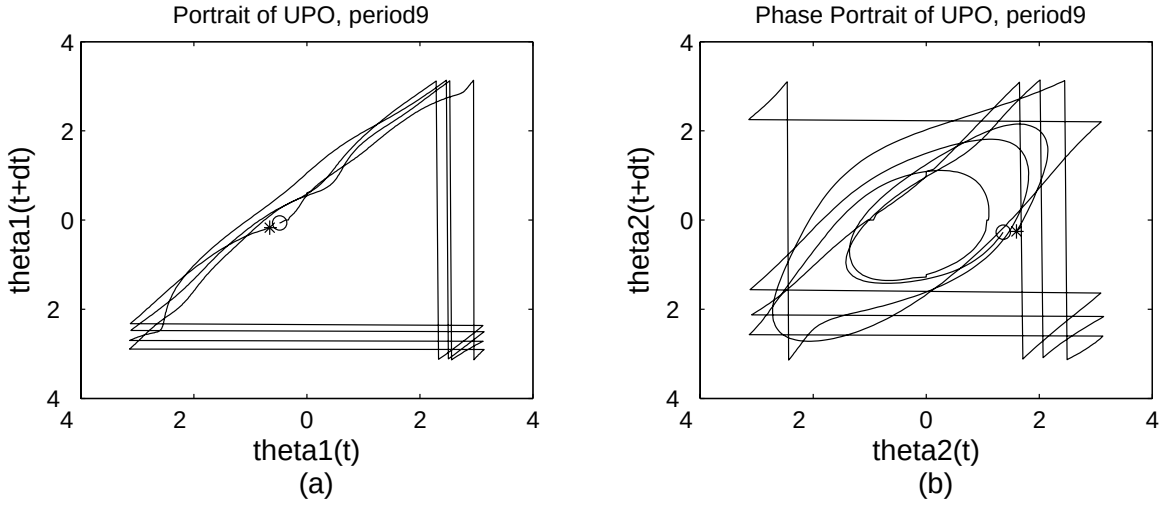

Figure 5: A period 9 UPO.

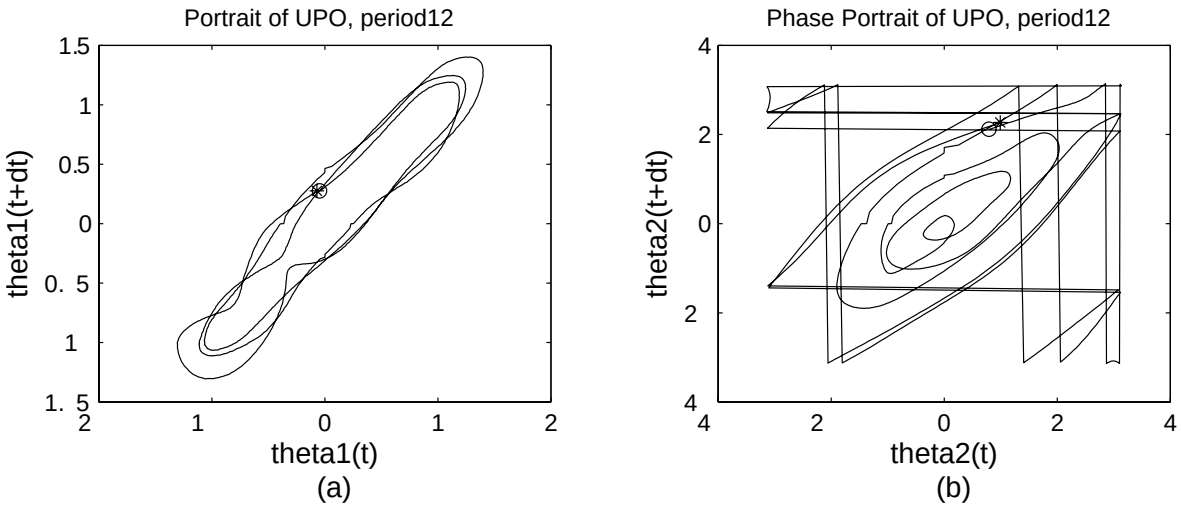

Figure 6: A period 12 UPO.

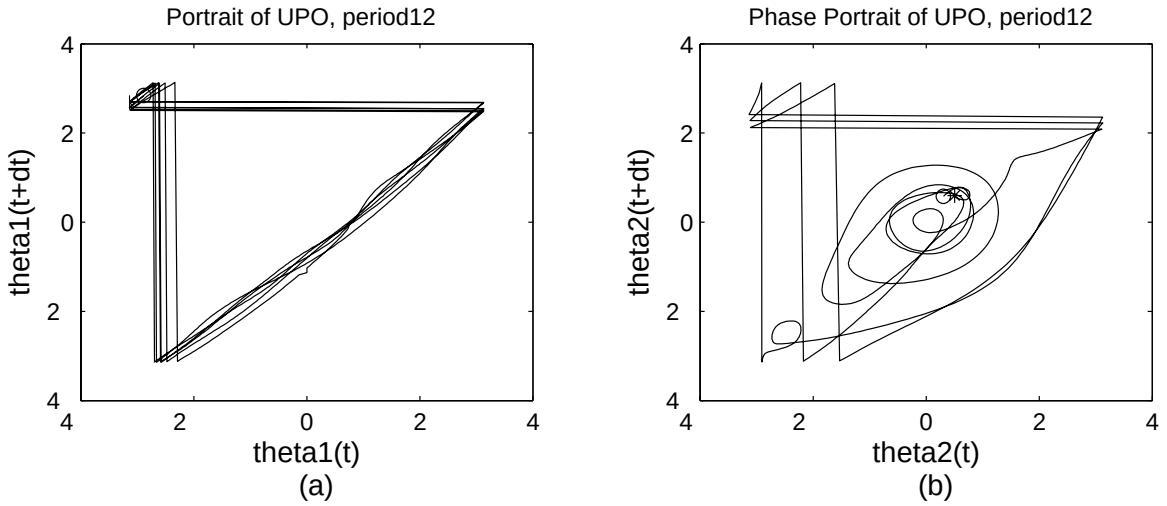

Figure 7: A period 12 UPO.

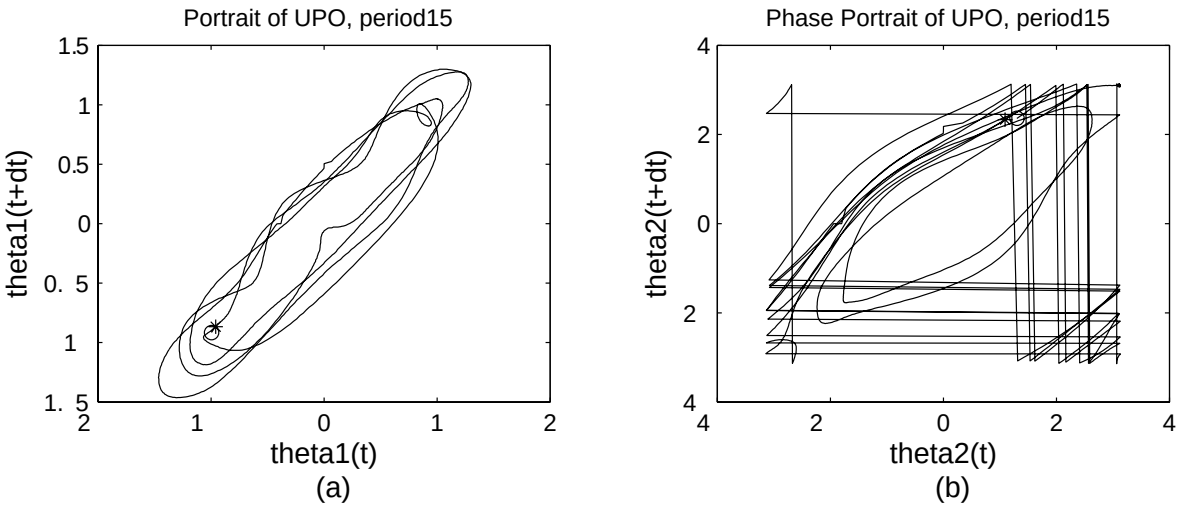

Figure 8: A period 15 UPO.

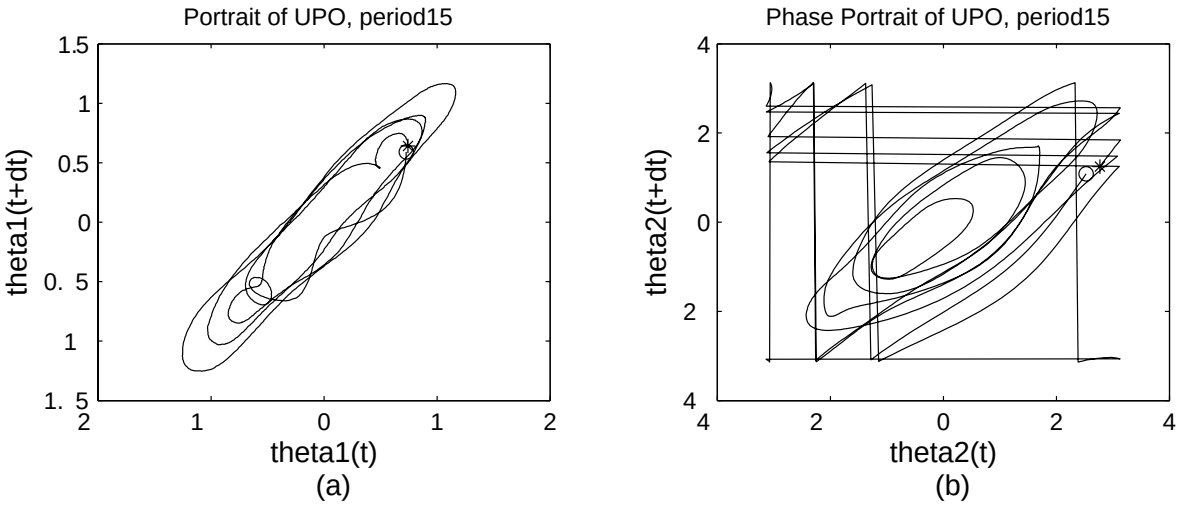

Figure 9: A period 15 UPO.

without whirling. Compared to [16, 17], the extracted UPOs in this double pendulum system are much fewer than the extracted UPOs in the single d. o. f. systems, which even had tolerance error smaller than 5%. This is probably because recurrences are less frequent in higher dimensional spaces for small periodicity k.

5.2 Identified parameters

Table 3 lists all of the identified parameters by Fourier series expansion of UPOs, applying Low-pass filter, FFT convolution, and harmonic balance method.

Table 3: Identified parameters by applying low-pass filter, FFT convolution, Fourier series expansion of UPOs, harmonic balance method with sub-harmonics whose frequencies are $\leq$ excitation frequency f_e=5 Hz, and sub-harmonics optimization.

–	**Identified values**	**True values**	**Error**×100%
B_{11}	0.1167	0.1131	3.2%
B_{12}	0.0781	0.0711	9.8%
B_{13}	0.0809	–	–
B_{14}	0.0264	–	–
$B_{15}=\sqrt{B_{13}^2+B_{14}^2}$	0.0849	0.0820	3.6%
B_{21}	1.6149	1.6816	4.0%
B_{22}	0.2562	0.2630	3.6%
B_{23}	0.2777	–	–
B_{24}	0.0715	–	–
$B_{25}=\sqrt{B_{23}^2+B_{24}^2}$	0.2868	0.2913	1.6%
C_{11} *	0.0001	1.02×10^{-3}	–
C_{12} *	0.0007	0.00366	–
C_2 *	0.0106	0.0485	–
J_{o1} (kg·m^2)*	5.8113×10^{-4}	5.99×10^{-4}	2.0%
J_{o2} (kg·m^2)*	4.1995×10^{-5}	4.033×10^{-5}	3.9%
a (cm)	1.18	1.15	2.6%
m_1e_1 (kg·m)	1.73×10^{-3}	1.60×10^{-3}	8.5%

The sub-harmonic terms whose frequencies are smaller than (or equal to) the excitation frequency were selected and optimized for identification purpose, because the noise is actually reduced in this frequency interval. The optimization process utilizes linear regression techniques and will be introduced later. The friction coefficients correspond to negative friction, or to energy generation, which is not physically realistic and therefore deemed inaccurate.

Part of the reason for this inaccuracy is due to the fact that both of the Coulomb friction and viscous damping factors are much smaller than other factors in the same matrix equations. However, despite the friction factors inaccuracy, most of other parameters match with the actual values within an error range of 10%, which is generally satisfying for experimental data.

Meanwhile, as we have mentioned before, some of the 'true' values (marked with '*') listed in Table 3 were obtained by indirect dynamical method, e. g. small angle free vibration, and thus those 'true' physical parameters and related non-dimensional parameters may also have some error. Thus, more verification methods were examined (see Section 5.6).

5.3 Friction issue

Our first result has showed that friction coefficients may not be precisely identified due to their small values. Previous researches [16, 17] also indicate that friction parameters were more difficult to identify accurately than other parameters in experiments for a single degree of freedom system. The inaccuracy can result from mainly three reasons:

1. experimental noise in sampled data;
2. inadequate sensor sensitivity (the resulted error can also be treated as a noise component);
3. inaccurate model of friction, e. g. viscous friction, dry friction, or their combination.

In the present experiment, the first two reasons affected the identification procedure. Furthermore, inadequate sensor sensitivity can actually be considered as one of the noise sources during data acquisition process. The noise decreases the accuracy of the extracted UPOs. As a result, the identified friction coefficients are erroneous, whereas other estimated parameters show only small discrepancies from the real values. What if the friction coefficients can be determined prior to identification, and therefore, the identification could be improved with the pre-knowledge of friction terms. Here, one would like to know the roles of friction parameters in the identification process, and whether the friction errors have influence on other identified parameters in the two-degree of freedom double pendulum system, which is slightly damped.

We can assume that friction parameters are already known, and we want to identify the other parameters in our harmonic balance method. In this work, we determined the friction in each pendulum bearing by a small amplitude free vibration method. The free vibration

test indicated that in the central arm, solely Coulumb friction was involved, and in the second arm, solely viscous friction was involved. The non-dimensional form of the friction parameters are listed in Table 1. Hence, we applied the identification algorithm with known friction coefficients.

Table 4: Identified non-dimensional parameters provided that the friction coefficients are known.

–	**Identified values**	**True values**	**Error**×100%
B_{11}	0.1178	0.1131	4.2%
B_{12}	0.0774	0.0711	8.8%
B_{13}	0.0829	–	–
B_{14}	0.0185	–	–
$B_{15} = \sqrt{B_{13}^2 + B_{14}^2}$	0.0852	0.0820	3.9%
B_{21}	1.6040	1.6816	4.6%
B_{22}	0.2646	0.2630	0.6%
B_{23}	0.2840	–	–
B_{24}	0.0483	–	–
$B_{25} = \sqrt{B_{23}^2 + B_{24}^2}$	0.2880	0.2913	1.2%

The result in Table 4 shows that the friction parameters, due to their much smaller values compared to other parameters (less than 1/5 of other parameters), have little influence on the overall result. This also implies that the small errors in other parameters can cause a large percent error in the friction terms. Hence, the first result in Table 3 is believed to be reliable for the coefficients of conservative and parametric excitation terms.

For further verification, a simulation of the double pendulum system based on equation (2) and the identified parameters was examined. However, unlike the robustness of the identification process, simulated double pendulum system is extremely sensitive to parameters' setting, e. g. friction parameters. The simulation was done under Matlab platform by digital integration. The simulation result was obtained (shown in Figure 10) under $C_{11} = 1.02 \times 10^{-3}$, $C_{11} = 0.00366$ and $C_2 = 0.0485$ and other parameters set as the identified values in Table 3.

5.4 High frequency noise in unstable periodic orbits

In the previous application of the chaotic system identification process [16, 17, 18] in which single d. o. f. systems were examined, the identification algorithm was noise resistant. How-

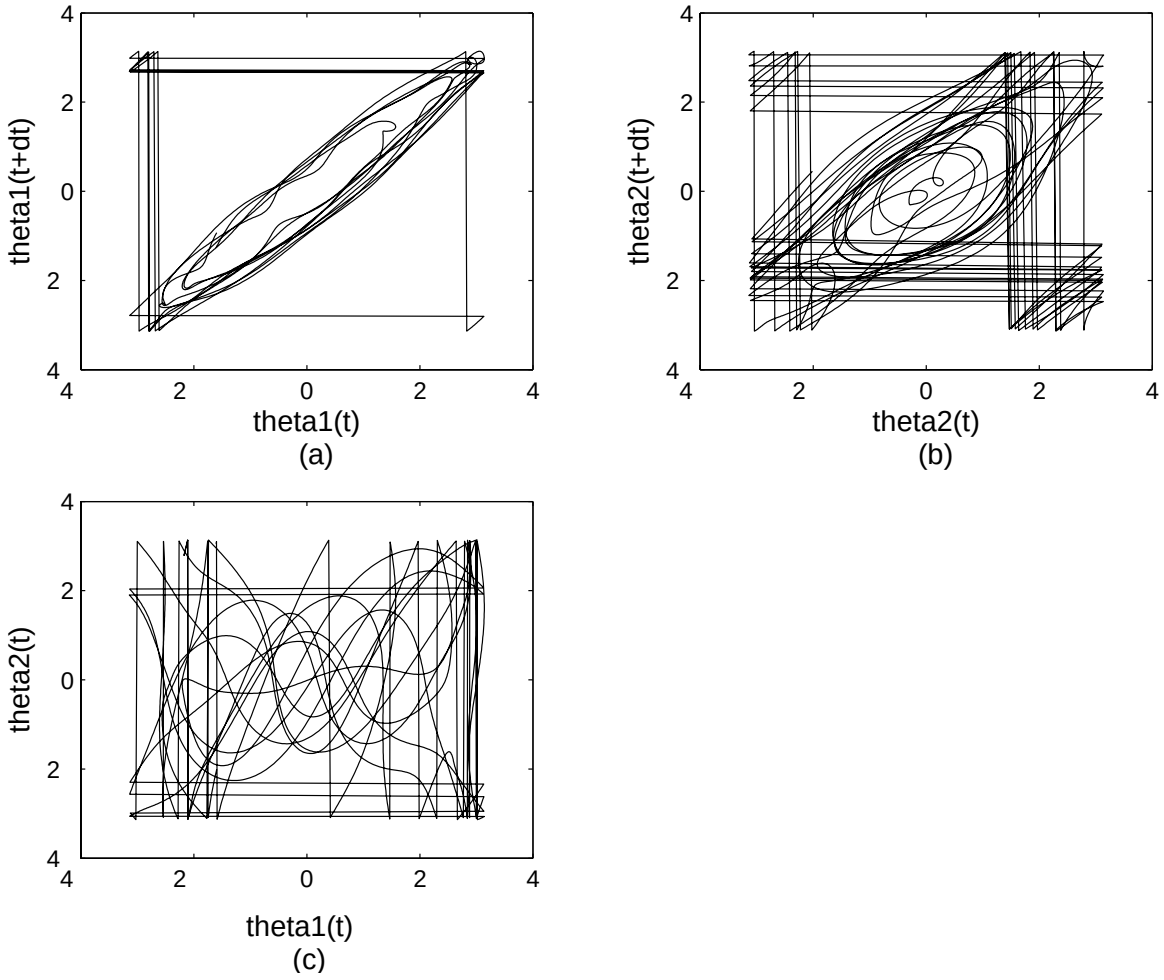

Figure 10: Phase portrait of the simulated system with $C_{11} = 1.02 \times 10^{-3}$, C_{11}=0.0366 and $C_2 = 0.0485$; dt=24.

ever, similar hypothesis could not be applied to the present two d. o. f. system. The reason is simply due to the strong non-linearity of the double pendulum, and it can be explained by the difference in the governing differential equations:

$$\ddot{\theta} + c/r\dot{\theta} + 1/r^2 \sin\theta - f \sin t \cos\theta = 0. \tag{25}$$

Equation (25) is the governing equation of a horizontally excited single pendulum, which was examined in [18]. Although the parametric excitation term is nonlinear, $\dot{\theta}$ and $\ddot{\theta}$ terms are, on the other hand, linear. The $\sin\theta$ term in (25) can also be regarded as linear in terms of harmonic functions. Suppose the contaminated signal is composed of the real signal and noise $n(t)$: $\theta(t) = \theta_t(t) + n(t)$. The angular speed and acceleration of periodic orbits can be obtained by equations similar to (7)–(10). Hence, the noise in the obtained speed and acceleration kth sub-harmonic is actually amplified by k, though $n(t)$ is rather small in the displacement signal. The overall signals of speed and acceleration are then considered to be contaminated mainly by high frequency noise. Apparently, to the system (25), where speed and acceleration terms are all linear, since in the identification matrix, only the first K terms of harmonic order are used, the high frequency noise whose frequency larger than $K+1$th harmonic term will be automatically filtered out, which explains why the identification process is noise resistant for systems like (25). Nevertheless, in the double pendulum system (4), the identification process appears to be less noise resistant than the previous examples since velocities and accelerations do not appear linearly in differential equations. Specifically, it is the $(\frac{d\phi_i}{d\tau})^2 \sin(\phi_2 - \phi_1)$ and $\phi_i'' \cos(\phi_2 - \phi_1)$ terms that contribute most to the noise inaccuracy of the result. Other high order terms also have similar problem of noise amplification. It can be explained by the following FFT equation

$$\mathcal{F}[\dot{\phi}_i^2 \sin(\phi_2 - \phi_1)] = \mathcal{F}(\dot{\phi}_i)^2 \otimes \mathcal{F}[\sin(\phi_2 - \phi_1)], \tag{26}$$

where $\mathcal{F}(x)$ represents the Fourier transform of x, and operator $\otimes$ represents convolution. The high frequency noise in each component is, therefore, mixed into the final result by convolution since convolution involves the integration of two signals. Furthermore, it actually amplifies the noisy influence of the angular displacement, e. g. high frequency noise, since in the algorithm, the frequency components of $\dot{\theta}_i$ and $\ddot{\theta}_i$ are obtained by equation (7)–(10). Hence, the truncation of the first K harmonic terms could not reduce the disturbance of the noise.

One way to avoid noise contamination is to filter out the high frequency noise of the signal after UPO extraction and before convolution. By doing so, the noise component can

be effectively controlled. The algorithm was incorporated in the identification process, and it turned out to be effective. Suppose $y = (\frac{d\phi_i}{d\tau})^2 \sin(\phi_2 - \phi_1)$, Table 5 compares the difference of the first 4 orders of Fourier series coefficients of y with low pass filtering before convolution and without filtering (shown in Figure 5). The cut-off frequency was set to be $1/5f_s$ Hz. Figure 11 shows the velocity and acceleration frequency spectra of θ_1. It can be seen that the acceleration's high frequency noise is quite intolerable, and even with the low pass filter of $1/5f_s$ cut-off frequency, there is still considerable noise remaining.

Table 5: Comparison of $\mathcal{F}(y)$ with and without filter added.

i	**Coefficients of** $\cos(ix)$		**Coefficients of** $\sin(ix)$	
	without filter	**with filter**	**without filter**	**with filter**
1	-3.2486	-0.3087	0.0328	0.0000
2	-34.0713	-27.1330	17.7370	17.7403
3	-15.6946	-8.6732	-23.6908	-23.2652
4	-31.2079	-24.1696	-10.2571	-10.6034

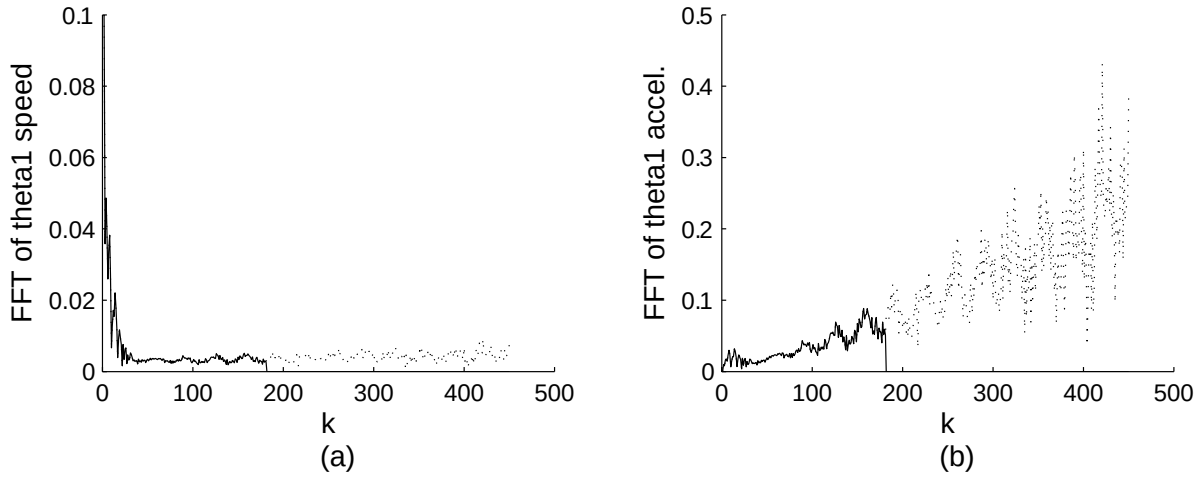

Figure 11: FFT amplitude of the $\dot{\theta}_1$ and $\ddot{\theta}_1$ with and without low pass filter applied; the continuous line is FFT of signals with filter of $1/5f_s$ cut-off frequency; the dotted line is FFT of signals without filter; k is the order of sub-harmonics.

Displayed in Figure 12 are also signals with and without the low pass filter for the period-9 UPO. The low pass filtered signals are more smooth and assumed to be closer to real signals. Meanwhile, an identification process without any filtering was examined

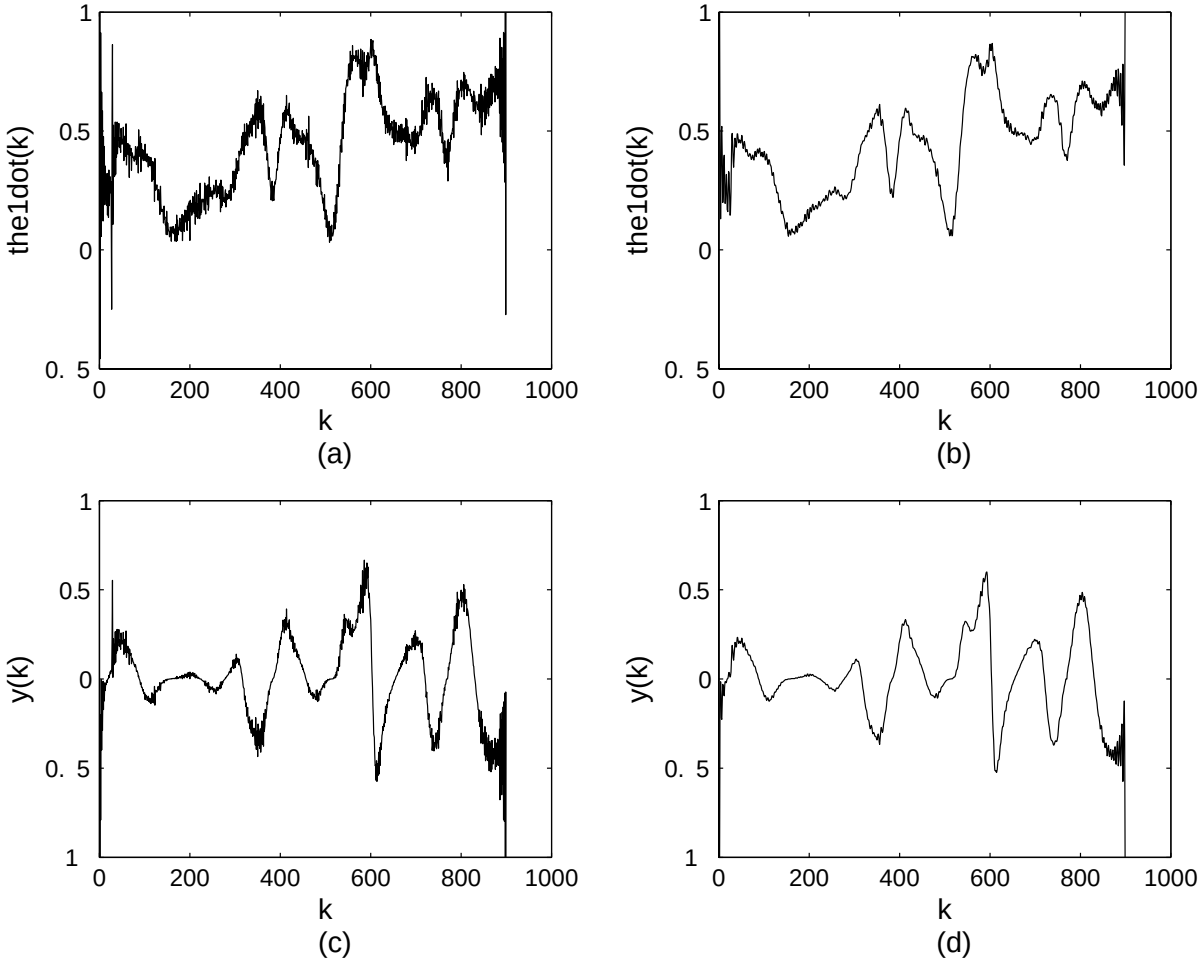

Figure 12: Signals without and with low pass filter applied; **a** and **b** are $\dot{\theta_1}$ without and with filter; **c** and **d** are y without and with filter applied to each convolution components; k is the kth sampled point of the orbit.

by utilizing the same periodic orbits displayed in Figures 4–9. Listed in Table 6 are the identified parameters. B_{21} displays a larger error because of the strong non-linearity of the related term and the relatively larger noise contamination level (due to θ_1's small oscillation amplitude and sensitivity of optical encoders).

Table 6: Optimized identification with no digital filter applied.

Parameters	**Identified values**	**True values**	**Error**$\times 100\%$
B_{11}	0.1125	0.1131	0.5%
B_{12}	0.0790	0.0711	11.1%
B_{15}	0.0825	0.0820	0.6%
B_{21}	1.1611	1.6816	31.0%
B_{22}	0.2553	0.2630	3.0%
B_{25}	0.2564	0.2913	12.0%
C_{11}	0.0003	1.02×10^{-3}	–
C_{12}	-0.0002	0.00366	–
C_2	0.0164	0.0485	–

5.5 Digital differentiation and error reduction

5.5.1 Recurrence tolerance

Due to the limited length of the experimental data, not many periodic orbits were extracted by setting the extraction error tolerance small, e. g. less than 5% in the present experiment. Thus, one would naturally tend to increase the error tolerance such that more periodic orbits can be extracted. However, with the increased error tolerance and hence more, but less accurate, periodic orbits, the identification results turned out to get worse for the double pendulum system. Table 7 lists the identified parameters (Fourier series method) with 8% error tolerance of extraction (in this case, 58 different orbits extracted), and showed large errors. For the present system, the coefficients B_{11} and B_{21} are parameters of strong nonlinear terms, and therefore, identification of these two parameters are usually less stable and more prone to get error.

The discrepancy comes mainly from large recurrence error, which resulted from the large error tolerance of UPO extraction. Figure 13 **a** and **b** display the calculated angular velocity and acceleration curves of a period-9 (Figure 5) orbit by means of Fourier series expansion method. It is showed that an impulse caused by recurrence error occurred in the periodic

Table 7: Comparison of calculated values by Fourier Series (FS) method and Digital Differentiation (DD) method when error tolerance is set as 8%.

Parameters	**FS ID**	**FS Error**×100%	**DD ID**	**DD Error**×100%
B_{11}	0.0126	88.5%	0.1224	8.2%
B_{12}	0.0730	2.7%	0.0760	6.9%
B_{15}	0.0908	10.7%	0.0908	10.7%
B_{21}	1.4703	12.6%	1.6103	4.3%
B_{22}	0.2607	0.9%	0.2559	3.7%
B_{25}	0.2851	2.1%	0.2772	4.8%
C_{11}	0.0014	–	-0.0003	–
C_{12}	0.0005	–	0.0016	–
C_2	0.0053	–	0.0093	–

speed and acceleration curve, which is not true for the real periodic orbits. If we look at the velocity curve, it can be express as

$$\dot{\hat{\theta}}(t) = \dot{\theta}(t) + \alpha\delta(t - t_c) + \eta(t), \tag{27}$$

where $\dot{\hat{\theta}}(t)$ is the calculated speed curve, $\dot{\theta}(t)$ is the real velocity curve, $\alpha\delta(t - t_c)$ is the impulse with amplitude α proportional to the recurrence error, t_c is time delay, and $\eta(t)$ is noise other than the recurrence one, which is considered to be small. Thus, after digital filtering, and applying Fourier transform, we obtain

$$\mathcal{F}(\dot{\theta}) \cong \mathcal{F}(\dot{\hat{\theta}}) + \alpha e^{-jt_c\omega}$$

, where α is the expression of the impulse function in frequency domain and is a white noise. Furthermore, this noise contaminates all the sub-harmonics of the velocity curve, which could not be eliminated by the low pass digital filter and could hence generate large error in the identification result.

5.5.2 Digital differentiation

Through the previous analysis, for large recurrence error, one would naturally consider that a similar scenario would happen to other dynamic systems with strong non-linearity. In this case, digital differentiation could be applied given adequate sampling points per cycle, e. g. a high sampling rate f_s. In this experiment, there were 100 points per excitation period.

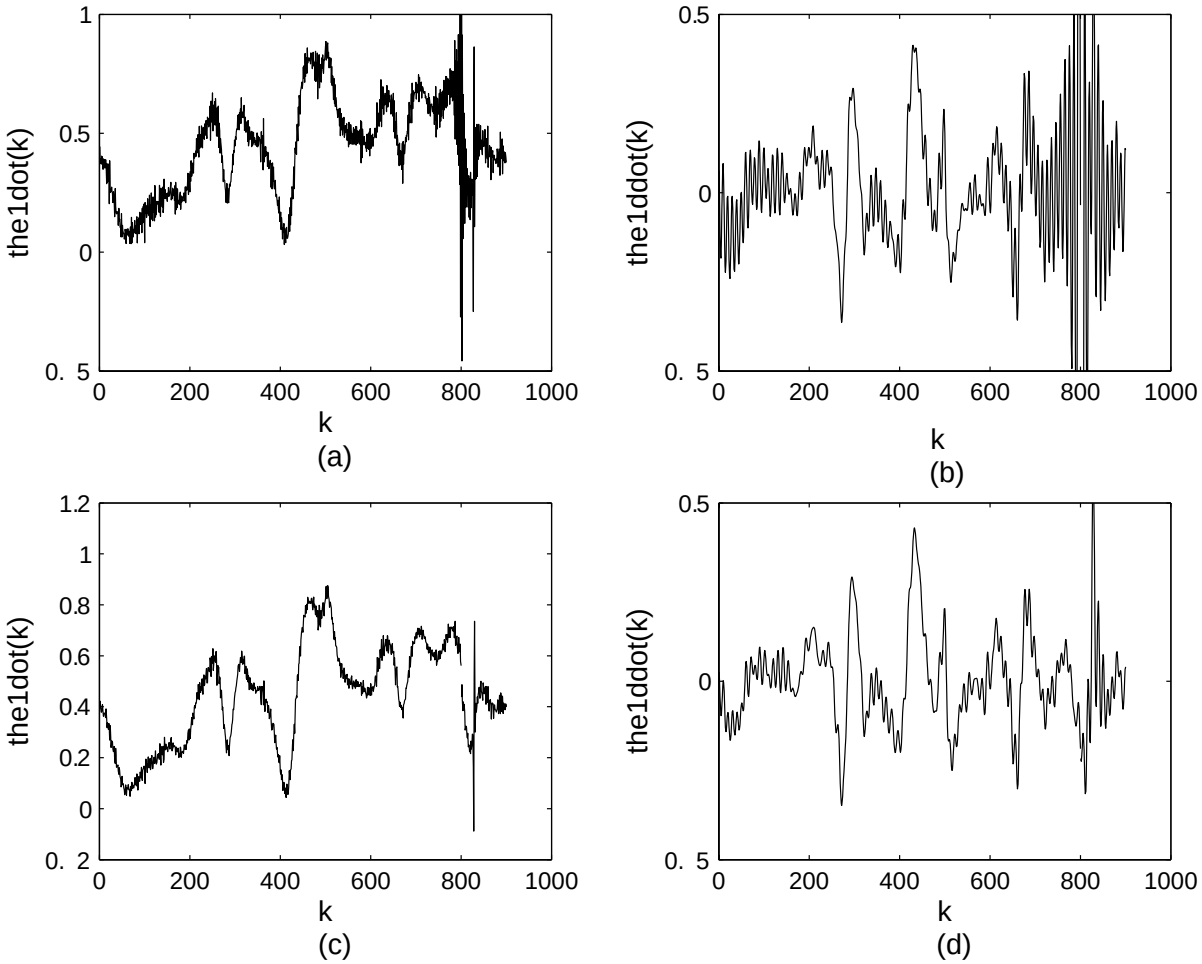

Figure 13: Obtained $\dot{\theta}_1$ and $\ddot{\theta}_1$ orbits by Fourier Series method (**a** and **b**) by digital differentiation method (**c** and **d**); the recurrence impulses occur at k=800 in (**a** and **b**.)

Hence, a five points differentiation algorithm was applied to obtain the derivatives and double derivatives of angular displacements:

$$\dot{f}(x) = \frac{8[f(x+h) - f(x-h)] - f(x+2h) + f(x-2h)}{12h} + o(h^4) \tag{28}$$

and

$$\ddot{f}(x) = \frac{16[f(x+h) + f(x-h) - 2f(x)] - f(x+2h) - f(x-2h) + 2f(x)}{12h^2} + o(h^4). \tag{29}$$

The errors of these algorithms can be reduced with a smaller time interval h. The five points algorithm can also reduce the influence of high frequency noise. The obtained curves are in Figure 13 **c** and **d** for the extracted period-9 orbit. It is apparent that the recurrence

impulses are eliminated for both of the cases, and much less high frequency noise displayed in the speed and acceleration curves. The corresponding identified parameters are listed in Table 7, which is more precise compared to the result of Fourier series method.

However, the algorithm of digital differentiation itself introduces calculation errors in equation (28) and (29). It could not predict precisely the small value parameters, e. g. friction parameters, according to a identification test based on the simulated double pendulum system. On the other hand, for the same simulated system, the Fourier series method can identify all of the parameters with satisfying accuracy if error tolerance of extraction is small enough (2% in this case). It shows that the digital differentiation method is more stable, but not more accurate compared to the Fourier series expansion algorithm.

5.5.3 Choice of sub-harmonics or harmonics

It was found that the identification result varied when a different choice of sub-harmonics was applied. The problem was not so troublesome in previous applications of the harmonic balance method [16, 17, 18] where nonlinearty is simple and not so strong as the double pendulum case. However, to the present experiment, different sub-harmonics set lead to quite different estimated parameters. It is then necessary for us to seek some general rules for judging whether the result.

In equation (18) and (20), the first M sub-harmonics of each UPO (sub-harmonics are functions of $\sin\left(\frac{ix}{k}\right)$ or $\cos\left(\frac{ix}{k}\right)$ where i and k represents the ith term in Fourier series of a period k orbit. The choice of M remains an issue. For a periodic orbit whose period is a multiple k of the excitation period, if $M \leq k$, i. e. sub-harmonics frequencies less than or equal to the driving frequency, the result was tested to be the best for the examined pendulum system. One reason is that these sub-harmonics consist of a large part of the displacement signals energy, and hence, contain relatively small portion of the noise contamination (see Figure 11). Also, the noise components in velocity and acceleration signals are reduced according to equations (7)–(10).

The remaining question is whether it is possible to measure the identification error and use it as an indicator of how 'true' the identification is. To quantify the identification error, we refer to linear regression techniques, borrow some concepts in statistics, and transform (18)–(22) into

$$\vec{e_i} = A_i\vec{\tilde{x}}_i - \vec{q_i}, i = 1, 2, \tag{30}$$

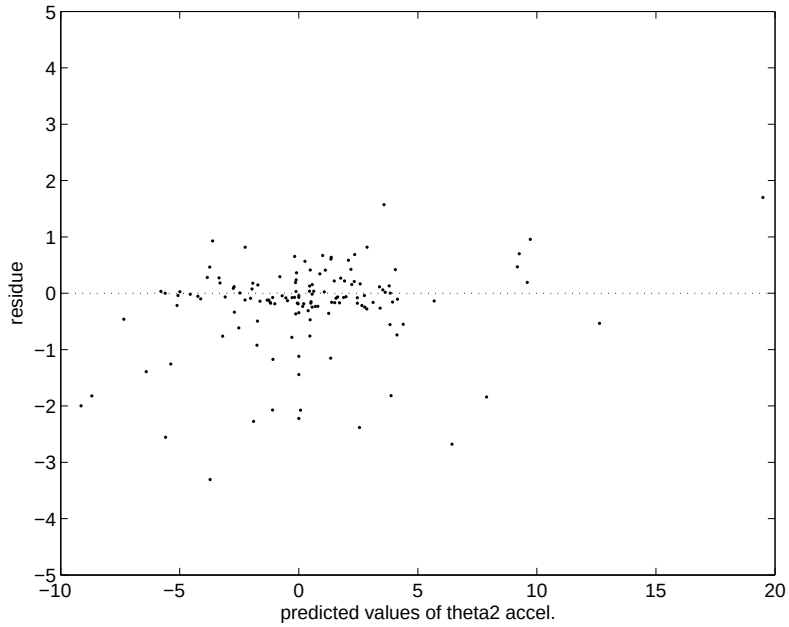

Figure 14: Identification residue of $\vec{e}_2$ with each dot representing a subharmonic; the horizontal position of each dot is the predicted value of $\vec{q}_2$, the vertical position of each point is the identification residue.

where $\vec{e}_i$ is the residue vector. Then, we can define the identification error ε_i as

$$\varepsilon_i = \frac{max(\|\vec{e}_i\|_\infty)}{max(\|\vec{\hat{q}}_i\|_\infty)},$$

where $\vec{\hat{q}}_i = A_i\vec{\hat{x}}_i$ is the predicted vector of $\vec{q}_i$. With the identification error defined, the rule of thumb for judging a good identification is $\varepsilon_i < \epsilon_c$, where ϵ_c is the positive critical value. $\epsilon_c = 10\%$ was used in the experiment. Figure 14 displays the residue $\vec{e}_2$ and the corresponding identification error ε_2 is 18.4% when all 140 sub-harmonics were included in the identification, whose frequencies were less than or equal to the driving frequency. Apparently, the results for B_{2j} for j=1, 2, 5, are not satisfying, and the comparison in Table 8 and Table 3 also corroborates the rule of thumb since B_{21} has a 11.2% error. On the other hand, The B_{1j} parameters have $\varepsilon_1 = 8.8\%$, and are quite consistent with the result after optimization in Table 3.

Our problem is now how to optimize the identification process so as to improve the accuracy, i. e. minimize the identification error. From the statistics point of view, we have a good linear regression curve if the resulting residues are distributed evenly and randomly around the predicted values. For this purpose, an optimization algorithm was developed to

Table 8: Identified parameters with no optimization to sub-harmonics set.

Parameters	**Identified**	**True values**	**Error**$\times 100\%$
B_{11}	0.1178	0.1131	4.2%
B_{12}	0.0782	0.0711	10.0%
B_{15}	0.0861	0.0820	5.0%
B_{21}	1.4935	1.6816	11.2%
B_{22}	0.2562	0.2630	0.5%
B_{25}	0.2828	0.2913	3.4%
C_{11}	0.0001	1.02×10^{-3}	–
C_{12}	0.0007	0.00366	–
C_2	0.0147	0.0485	–

exclude the sub-harmonics terms which result in large residues, and retain the good terms, which consist of most of the sub-harmonics and should have small residues. It involves the following steps:

1. Given the set of sub-harmonics, do the identification process and find out the maximum absolute residue value e_{max}.

2. For a level of significance β, which is a small value, remove from the sub-harmonics set those sub-harmonics whose corresponding residue $e > (1 - \beta)e_{max}$.

3. Repeat the first step by using the remaining sub-harmonics, and compute the identification error ε_i.

4. If $\varepsilon_i < 10\%$, then stop the optimization process and assume that the desired result has been obtained; if not, go back to step 1 with the remaining sub-harmonics set and repeat the optimization process.

For the investigated system, after 3 optimization processes with $\beta = 5\%$ (by excluding 10 erroneous sub-harmonics), the identification errors are reduced to $\varepsilon_1 = 8.1\%$ and $\varepsilon_2 = 9.4\%$. The corresponding results are listed in Table 3. Displayed in Figure 15 is the residue distribution of $\vec{e_2}$ after optimization. Compared to the identified values without optimization in Table 8, the optimized ones have smaller errors and are more accurate. However, the proposed optimization can not work well for all cases. If after a few times of optimization, the identification errors are still undesirable, we should either use more precise UPOs, or re-select the set of sub-harmonics before optimization such that the noise contamination can be

minimized. In order to obtain more precise UPOs, besides the UPO extraction with smaller tolerance of error, we can also refine the extracted UPOs [19]. But the refinement process may generate erroneous results for quasi-periodic orbits and not adequate for limited data set. For better selection of sub-harmonics, one may choose only those sub-harmonics that have the largest amplitude in the UPOs' acceleration FFT spectrum (also avoid those noise contaminated high frequency sub-harmonics, since it could only be noise). Furthermore, the selection could be simplified by choosing the harmonics instead of sub-harmonics if most of the orbits are composed mainly of the harmonics of the driving frequency f_e.

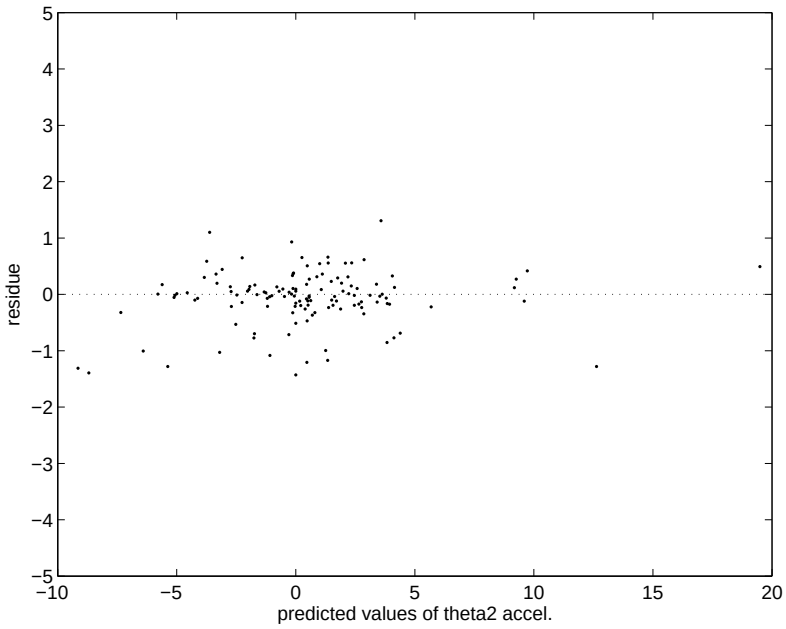

Figure 15: Identification residue after optimization for $\vec{e}_2$ with each dot representing a sub-harmonic.

5.6 Validation methods

Generally, most of the parameters of a nonlinear system are unknown to us. The direct comparison discussed in previous sections is not available for most applications. Besides, lots of the 'true' parameters in Table 1 were also estimated. Hence, we are not clear what the exact errors are for the identified values. Two other methods were applied here to verify the identified parameters and the effectiveness of the identification algorithm. The first one is to verify our method by identifying the simulated double pendulum system such that comparisons can be made based on identification results and the phase portraits of

the experimental and simulated systems. The second method involves the linearized system properties, e. g. natural frequencies.

5.6.1 Identification of the simulated double pendulum system

To verify the effectiveness of identification process, a simulated system was also examined with parameters setting as the identified values listed in Table 3 except for the friction terms (see Section 5.3). The error tolerance of extracting unstable periodic orbits is 5%. The phase portrait has been shown in Figure 10. Some similarity observed in the simulated system compared to the experimental phase portrait (displayed in Figure 3), e. g. chaotic behavior. Many detailed chaotic charasteristics were not available due to the inadequate experiment data. However, it turned out that more and different UPOs could be extracted from the equally large, sampled data of the simulated system , than from the experimental data set. Meanwhile, for the simulated system, the comparison in Table 9 between the identified values

Table 9: Comparison of the identified values and the true parametric settings of the simulated system.

–	**Identified**	**Parameters setting**	**Error**×100%
J_{o1} (kg.m^2	5.767×10^{-4}	5.757×10^{-4}	0.2%
J_{o2} (kg.m^2	4.310×10^{-5}	4.228×10^{-5}	1.0%
B_{11}	0.1166	0.1167	0.1%
B_{12}	0.0787	0.0781	0.8%
B_{15}	0.0848	0.0849	0.1%
C_{11}	0.0005	0.0	–
C_{12}	0.0038	0.00366	3.8%
B_{21}	1.5943	1.6149	1.3%
B_{22}	0.2568	0.2562	0.2%
B_{25}	0.2866	0.2868	0.1%
C_2	0.0429	0.0485	11.5%

and the parameter settings shows that all the parameters including the friction coefficients are identified correctly, which confirms the effectiveness of this algorithm. The friction coefficients, probably due to their much smaller values and the weakness of the least mean square method, are still hard to calculate very accurately, and thus, identified with larger error percentages. With little noise in the simulated data, the error can only come from the recurrence error of the extracted periodic orbits. Also, it confirms the difficulty of identify

small friction parameters in the experiment, since more noise contamination occurred in the experimental data.

5.6.2 Linear properties

The linearized pendulum can also be applied to validate the identification results, e. g. comparing the natural frequencies of the linearized system. Suppose the pendulum has only small angle oscillation without excitation force, by discarding the higher order terms and neglecting dry friction, equation (4) can be simplified to

$$\begin{cases} \frac{d^2\phi_1}{d\tau^2} + B_{11}\frac{d^2\phi_2}{d\tau^2} + B_{12}\phi_1 - C_{12}(\dot{\phi}_2 - \dot{\phi}_1) = 0 \\ \frac{d^2\phi_2}{d\tau^2} + B_{21}\frac{d^2\phi_1}{d\tau^2} + B_{22}\phi_1 - C_2(\dot{\phi}_2 - \dot{\phi}_1) = 0 \end{cases} . \tag{31}$$

Since our goal is to examine the natural frequencies, by neglecting the damping terms, equation (31) can be further simplified to the form of

$$\begin{cases} \frac{d^2\phi_1}{d\tau^2} = \frac{-B_{12}}{1-B_{11}B_{21}}\phi_1 + \frac{B_{22}B_{11}}{1-B_{11}B_{21}}\phi_2 \\ \frac{d^2\phi_2}{d\tau^2} = \frac{B_{12}B_{21}}{1-B_{11}B_{21}}\phi_1 + \frac{-B_{22}}{1-B_{11}B_{21}}\phi_2 \end{cases} , \tag{32}$$

and the characteristic matrix of equation (32) is

$$A = \begin{pmatrix} 0 & 1 & 0 & 0 \\ \frac{-B_{12}}{1-B_{11}B_{21}} & 0 & \frac{B_{22}B_{11}}{1-B_{11}B_{21}} & 0 \\ 0 & 0 & 0 & 1 \\ \frac{B_{12}B_{21}}{1-B_{11}B_{21}} & 0 & \frac{-B_{22}}{1-B_{11}B_{21}} & 0 \end{pmatrix} . \tag{33}$$

The eigenvalues of matrix A are the natural frequencies of the linearized system in non-dimensional form. The natural frequencies of the identified system were solved to be 1.336Hz and 2.904Hz. Through FFT analysis, the natural frequencies obtained by experimental data are 1.25Hz and 3.00Hz. Comparison in Table 10 shows that the natural frequencies match with the FFT result. It shows that the identified parameters excluding the friction terms are reliable for the purpose of system linearization.

Table 10: Natural frequencies.

–	**Identified**	**Experimental**	**Error** $\times$ 100%
f_{n1}	1.336	1.25	6.9%
f_{n2}	2.904	3.00	3.2%

6 Conclusions

A double pendulum system experiment was examined for chaotic system identification. The investigated system was a multi-degree of freedom system with strong non-linearity, e. g. mixed ϕ_i, $\dot{\phi}_i$ and $\ddot{\phi}_i$ non-linearity. However, only displacement signals were directly measured data. To adapt to these new challenges, some modifications were added in the harmonic balance identification algorithm:

1. The identification appeared to be less noise-resistant in this case, mainly due to the strong nonlinear term of $(\frac{d\phi_i}{d\tau})^2 \sin(\phi_2 - \phi_1)$ and $\phi_i'' \cos(\phi_2 - \phi_1)$. The high frequency noise contaminated the strong nonlinear terms without adequate low pass filtering of each component before convolution.

2. Digital differentiation algorithm was developed and applied to the experiment data in order to make the identification results more robust even with large recurrence errors in the extracted orbits. It could be of use for limited data set. However, the digital differentiation algorithm also introduced differentiation error, and thus, did not give accurate values of friction terms.

3. Choices of sub-harmonics terms also had influence on the identified parameters. Inappropriate selection of sub-harmonics can generated poor results. To avoid poor results, the key factor was to avoid noise contaminated sub-harmonics. For the present system, the subharmonics with frequency less than excitation frequency were selected to avoid noise.

4. Linear regression techniques were applied to quantify the identification error ϵ_i, which reflected the error of the identified parameters by examining the residues and the predicted values. Based upon the identification error, an optimization algorithm was proposed to improve the result. An identification error less than 10% indicated an rather satisfying result. However, optimization is limited by its statistical property, and can not work for all data to satisfy the rule of thumb.

Friction was a problem in the identification process. For slightly damped systems, since the friction factors were much smaller than other parameters, the identification could not produce accurate values of the friction terms. Noise and recurrence error were the two factors that contributed to this error. However, the harmonic balance algorithm is robust, and the

validation process showed that the friction error had little effect on other identified parameters. Through the experiment, it can be concluded that the examined identification method can be applied to systems of chaotic, strong non-linearity and multi-degree of freedom. With adequate modification, the identification result could be improved, and the quality of the result can be quantified by the identification error.

References

[1] M. R. Hajj and A. H. Nayfeh, et al. 1985, "Parametric Identification of nonlinear dynamic systems", *Computers & Structures*, Vol. 20 (1-3), pp. 487–493.

[2] M. R. Hajj, J. Fung, A. H. Nayfeh and S. O. Fahey, 1986, "Damping identification using perturbation techniques and higher order spectra", *Nonlinear Dynamics*, Vol. 23(2), pp. 189–203.

[3] Q. Chen and G. R. Tomlinson, 1996, "Parametric identification of systems with dry friction and nonlinear stiffness a time series model", *Journal of Vibration and Acoustics*, Vol. 118(2), pp. 252–263.

[4] R. K. Kapania and S. Park, 1997, "Parametric identification of nonlinear structure dynamic systems using finite element method", *AIAA Journal*, Vol. 35(4), pp. 719-726.

[5] R. Ghanem and F. Romeo, 2001, "A wavelet-based approach for modal and parameter identification of nonlinear systems", *International Journal of nonlinear mechanics*, Vol. 36(5), pp. 835–859.

[6] O. Gottlieb and M. Feldman, 1997, "Application of a Hilbert-transform based algorithm for parameter estimation of a nonlinear ocean system roll model", *Journal of Offshore Mechanics and Arctic Engineering*, Vol. 119, pp. 239–243.

[7] M. Feldman, 1997, "Nonlinear free vibration identification via the Hilbert transform", *Journal of Sound and Vibration*, Vol. 208(3), pp. 475–489.

[8] N. B. Tufillaro, T. Abbott and J. Reilly, 1992, "An experimental approach to nonlinear dynamics and chaos", *Addison-Wesley*.

[9] D. Auerbach, P. Cvitanovic, J. P. Eckmann, G. Gunaratne and I. Procaccia, 1987, "Exploring chaotic motion through periodic orbits", *Physical review Letters*, Vol. 58, pp. 2387–2389.

[10] D. P. Lathrop and E. J. Kostelich, 1989, "characterization of an experimental strange attractor by periodic orbits", *Physical Review A*, Vol. 40, pp. 4028–4031.

[11] H. D. I. Abarbanel, R. Brown, J. J. SIDorowich and L. S. Tsimring2, 1993, "The analysis of observed chaotic data in physical systems", *Reviews of Modern Physics*, Vol. 65, pp. 1331–1392.

[12] K. Yasuda, S. Kawamura and K. Watanabe, 1998, "Identification of nonlinear multi-degree-of-freedom systems (presentation of an identification technique)", *JSME International Journal, Series III*, Vol. 31, pp. 8-14.

[13] K. Yasuda, S. Kawamura and K. Watanabe, 1998, "Identification of nonlinear multi-degree-of-freedom systems (identification under noisy measurements)", *JSME International Journal, Series III*, Vol. 31, pp. 302-309.

[14] N. P. Plakhtienko, 2000, "Methods of identification of nonlinear mechanical vibrating systems", *International Applied Mechanics*, Vol. 36 (12), pp. 1565-1594.

[15] N. P. Plakhtienko, 1983, "A method of special weight-functions in the problem of parametric identification of mechanical systems", *DOPOV AKAD NAUK A*, Vol. 8, pp. 31-35.

[16] C. M. Yuan and B. F. Feeny, 1998, "Parametric Identification of Chaotic Systems", *Journal of Vibration and Control*, Vol. 4 (4), pp. 405-426 .

[17] B. F. Feeny, C. M. Yuan and J. P. Cusumano, 2001, "Parametric identification of an experimental magneto-elastic oscillator", *Journal of Sound and Vibration*, Vol. 247 (5), pp. 785-806.

[18] Y. Liang and B. F. Feeny, 2003, "Parametric identification of chaotic systems, Part I: parametric identification of a simulated horizontally excited pendulum", *Appendix A*.

[19] Z. Al-Zamuel, B. F. Feeny, 2001, "Improved estimations of unstable periodic orbits extracted from chaotic sets", *2001 ASME Design Engineering Technical Conferences, Proceedings of DET'01*.